New Technique for Quantification of Elemental Hg in Mine Wastes and Its Implications for Mercury Evasion Into the Atmosphere

ARTICLE *in* ENVIRONMENTAL SCIENCE & TECHNOLOGY · JANUARY 2011

Impact Factor: 5.33 · DOI: 10.1021/es1023527 · Source: PubMed

5 AUTHORS, INCLUDING:

Christopher Kim
Chapman University
35 PUBLICATIONS **1,379** CITATIONS

SEE PROFILE

J. J. Rytuba
U S Geological Survey Menlo Park
73 PUBLICATIONS **1,650** CITATIONS

SEE PROFILE

Published in final edited form as:
Environ Sci Technol. 2011 January 15; 45(2): 412–417. doi:10.1021/es1023527.

A New Technique for Quantification of Elemental Hg in Mine Wastes and Its Implications for Mercury Evasion Into the Atmosphere

ADAM D. JEW[1,*], **CHRISTOPHER S. KIM**[2], **JAMES J. RYTUBA**[3], **MAE S. GUSTIN**[4], and **GORDON E. BROWN JR.**[1,5]

[1] Surface and Aqueous Geochemistry Group, Department of Geological & Environmental Sciences, Stanford University, Stanford, CA 94305-2115, USA

[2] Environmental Geochemistry Lab, Department of Chemistry, Chapman University, One University Drive, Orange, CA 92866, USA

[3] USGS Mineral Resources Program, U.S. Geological Survey, 345 Middlefield Road, MS 901, Menlo Park, CA 94025, USA

[4] Department of Natural Resources and Environmental Science, University of Nevada, Reno, NV 89557, USA

[5] Department of Photon Science and Stanford Synchrotron Radiation Lightsource, SLAC National Accelerator Laboratory, 2545 Sand Hill Road, MS 69, Menlo Park, CA 94025, USA

Abstract

Mercury in the environment is of prime concern to both ecosystem and human health. Determination of the molecular-level speciation of Hg in soils and mine wastes is important for understanding its sequestration, mobility, and availability for methylation. Extended x-ray absorption fine structure (EXAFS) spectroscopy carried out under ambient P-T conditions has been used in a number of past studies to determine Hg speciation in complex mine wastes and associated soils. However, this approach cannot detect elemental (liquid) mercury in Hg-polluted soils and sediments due to the significant structural disorder of liquid Hg at ambient-temperature. A new sample preparation protocol involving slow cooling through the crystallization temperature of Hg(0) (234K) results in its transformation to crystalline α-Hg(0). The presence and proportion of Hg(0), relative to other crystalline Hg-bearing phases, in samples prepared in this way can be quantified by low-temperature (77K) EXAFS spectroscopy. Using this approach, we have determined the relative concentrations of liquid Hg(0) in Hg mine wastes from several sites in the California Coast Range and have found that they correlate well with measured fluxes of gaseous Hg released during light and dark exposure of the same samples, with higher evasion ratios from samples containing higher concentrations of liquid Hg(0). Two different linear relationships are observed in plots of the ratio of Hg emission under light and dark conditions vs. % Hg(0), corresponding to silica-carbonate- and hot springs-type Hg deposits, with the hot springs-type samples exhibiting higher evasion fluxes than silica-carbonate type samples at similar Hg(0) concentrations. Our findings help explain significant differences in Hg evasion data for different mine sites in the California Coast Range.

[*]Corresponding author: adamjew@stanford.edu.

Supplemental Materials Available. This information is available free of charge via the internet at http://pubs.acs.org/

Introduction

Mercury is a widespread global pollutant that is highly toxic in certain forms to both humans and aquatic ecosystems (1). Significant sources of Hg impacting ecosystems in California include areas containing inoperative mercury mines, such as New Almaden and New Idria, as well as several thousand smaller Hg mines occurring throughout the California Coast Range (2) and placer Au deposits in the Sierra Nevada foothills and the Klamath-Trinity Mountains of California (3). The potential bioavailability and toxicity of mercury vary dramatically depending on its speciation (4), and thus it is important to have detailed knowledge of Hg speciation in Hg-polluted sediments and mine wastes in order to determine a site's potential environmental hazard.

Common methods for determining Hg speciation in contaminated materials include sequential chemical extractions (SCE) (5), pyrolysis measurements (6), extended x-ray absorption fine structure (EXAFS) spectroscopy (7–9), and transmission electron microscopy (TEM) coupled with energy dispersive analysis (10,11). SCEs and pyrolysis are both indirect methods that are destructive to the samples and subject to varying interpretation (12–13). Although SCEs are widely used to estimate Hg speciation in contaminated soil and sediment samples (e.g., (5)), SCEs can cause new Hg species to form as a result of the chemical treatments (10). Pyrolysis causes thermal desorption of Hg with increasing temperature, and the amount released at different temperatures can be measured (6,14–16). Two problems in using pyrolysis for Hg speciation are that different Hg species can have overlapping release temperatures making quantification difficult, and it is destructive to the sample. In contrast, EXAFS spectroscopy is a direct, non-destructive method for determining Hg speciation, when Hg concentrations are above 50 ppm, but up to this point, it has not been capable of detecting liquid Hg(0) in complex Hg-polluted samples. TEM analysis requires an ultra-high vacuum sample environment, which can result in dehydration of the sample and potential loss of volatile Hg species, such as Hg(0). In addition, sampling is statistically limited during TEM analysis because of the relatively small amount of sample examined.

Ambient-temperature EXAFS studies of Hg mine wastes and associated sediments have shown that Hg is primarily in the form of cinnabar (α-HgS) and/or metacinnabar (β-HgS) with minor proportions of highly soluble Hg salts (7,17). Other EXAFS studies of Hg-impacted gold placer mining deposits have shown that even though liquid Hg(0) was used during the recovery of fine-grained Au, mainly colloidal HgS was detected and presumably formed during Hg transport through watersheds (18). However, because Hg is a liquid and thus disordered at ambient-temperature and pressure, these past EXAFS studies were unable to detect liquid Hg(0) in Hg-impacted mine wastes and sediments. Here we report a new protocol for converting liquid Hg(0) in such samples into a crystalline form (α-Hg) by slow cooling through its crystallization temperature of −38.83°C (234K). We show that it is possible to determine quantitatively the percentage of liquid Hg(0) in complex Hg-polluted samples prepared by this protocol using low-temperature (77K) EXAFS spectroscopy. Based on past experience, we estimate that a Hg concentration ≥ 50 ppm is required for detecting liquid Hg(0) using this approach in Hg mine wastes and associated Hg-polluted sediments and soils.

Studies of Hg evasion from Hg-impacted sediments and Hg mine wastes have shown significant differences in the amount of gaseous Hg released from a given sample when it is exposed to light versus dark conditions (19). Gustin *et al*. hypothesized that photoreduction of Hg(II) in Hg-containing sulfide, chloride, and oxide phases to elemental Hg causes these differences, with samples containing corderoite ($Hg_3S_2Cl_2$), metacinnabar (β-HgS), and Hg bound to organic and inorganic phases exhibiting higher light-enhanced emissions relative to

samples containing predominantly cinnabar (19). What was not known in this earlier study, however, is that significant quantities of Hg(0) were present in some of the samples studied (*e.g.*, from the Sulphur Bank Mercury Mine, Clear Lake, CA) which cannot be accounted for by photoreduction alone. Here we show that the concentrations of liquid Hg(0) in Hg-polluted soils, sediments, and mine wastes from the California Coast Range determined using this new sample preparation protocol and low-temperature EXAFS spectroscopy can help explain light-enhanced emission of Hg as measured on similar samples under controlled light and dark conditions.

Experimental Section

Samples and Mercury Concentration Measurements

Samples of mine waste and calcine material were collected in 2004 from the Knoxville, New Almaden, New Idria, and Sulphur Bank mines (all located in the California Coast Range) were collected and separated, using stainless steel sieves, into a number of different size fractions in the laboratory, from which 500–2000μm, 75–125μm, and <45μm diameter size fractions were selected for additional study. The selected size fractions were split into three sets for (1) analysis of total Hg concentrations, (2) Hg volatilization experiments, and (3) ambient- and low-temperature EXAFS studies. One split was sent to ChemEx Laboratories (Sparks, NV) to determine total Hg concentration by aqua regia digestion and cold vapor atomic fluorescence spectrometry (CVAFS) following US EPA method 1631, which has estimated error limits of 5–10% (20). Another split was used in Hg volatilization experiments under controlled light-dark conditions at the University of Nevada-Reno. Hg flux was measured for waste materials using a single pass gas exchange system at 35°C, a Tekran® 2537A CVAFS, and a Tekran® automated dual sampling unit (19). Samples were allowed to equilibrate in the chamber 24 h before data collection. Hg flux was calculated using the following equation:

$$F=Q(C_o - C_i)/A$$

where F is the total flux in ng Hg/m^{2}h; C_o and C_i are the Hg concentration of outlet and inlet air in ng Hg/m^3, respectively; A is the surface area of substrate in m^2; and Q is the flow of air through chamber in m^3/h (19). The third split was used for low temperature EXAFS spectroscopy analysis employing the new sample preparation protocol described below. Following the initial ambient-temperature EXAFS study of the field samples by Kim *et al.* (7), they were stored in the dark at constant temperature (25°C) in the original sample holders until the new slow cooling sample preparation protocol and low-temperature EXAFS study were carried out four years later. Storage at 298K and the use of a Teflon® sample holder sealed with Kapton® tape should have minimized liquid Hg(0) volatilization during storage. Storage in the dark should have prevented photoreduction of the samples from occurring. Such sample storage conditions should have minimized any changes in the Hg phases present in the samples over time.

EXAFS Methods

Low-temperature (77K) EXAFS spectra were collected at the Stanford Synchrotron Radiation Lightsource (SSRL) on wiggler beamline 11-2 using a LN_2-cooled Si (220) monochromator in the phi = 90° orientation. Spectra for all field samples and α-Hg(0) (due to sample thickness) were collected in fluorescence mode using a 30-element Ge detector, whereas spectra for all other Hg reference materials were collected in transmission mode using three ion chambers (one before and two after the sample). A $HgCl_2$ reference foil was placed between the second and third ion chamber for continuous energy calibration; it was placed directly in front of the third ion chamber, which was separated from the second ion

chamber by 7 cm to minimize a Hg-fluorescence signal from the energy calibration standard in the second ion chamber. When α-Hg(0) EXAFS spectra were collected, the SSRL storage ring was at an energy of 3.0 GeV and a current of ~90 mA, with an x-ray beam size collimated to 1mm × 1mm. An aluminum filter was placed between the sample and the Ge detector to minimize fluorescence signals from lighter elements into the detector. The incident x-ray beam was detuned by 30% to reduce higher order harmonics. An aluminum cold finger LN_2 cryostat was used to slowly freeze samples for the low-temperature (77K) EXAFS studies. An α-Hg(0) reference sample was prepared by very slow cooling of a liquid Hg(0) sample through its crystallization temperature of −38.83°C in a 1.5mm thick Teflon® holder sealed with Kapton® tape. Plunging the sample into a LN_2 bath, as is typically done prior to inserting a sample into a liquid-He cryostat for EXAFS work at 10K, results in production of amorphous solid Hg(0), which has an EXAFS spectrum similar to that of Hg(0) in the liquid form. To ensure that well-ordered α-Hg(0) was produced, we pre-cooled the cryostat (described below) and used a Teflon® sample holder because Teflon® has a low thermal conductivity (0.221W/mK) (21) and it does not react with Hg(0).

Before EXAFS data collection for the α-Hg(0) reference sample, the cryostat was first pre-cooled so that the reference sample could slowly cool and begin crystallizing while the sample chamber was evacuated. Cooling was accomplished by filling the empty cryostat with LN_2 to cool the cold finger to 77K. Once this was achieved, the LN_2 was removed, and the cold finger block was heated with a heat gun until the ice build up on the Al block of the cold finger had just started melting. After wiping away the accumulated water, the liquid Hg(0) sample was attached to the Al block with Kapton® tape, then the sample chamber was immediately evacuated for 20 minutes. Because the empty LN_2 reservoir of the cryostat was still near 77K, the sample cooled much more slowly than if the reservoir had been filled with LN_2, resulting in crystallization instead of quenching to an amorphous solid. Once the sample chamber was fully evacuated, LN_2 was slowly added by pouring ~100mL of LN_2 into the reservoir at 5 minute intervals for a half hour then finally filling the reservoir completely with LN_2.

Previous attempts at freezing the sample faster resulted in the production of Hg(0) glass that had an EXAFS spectrum very similar to that of liquid Hg(0) at ambient temperature, which is characterized by low amplitude oscillations. Reference samples of α-HgS, β-HgS, HgO, $HgCl_2$, $HgSO_4$, and HgSe were purchased from Alfa Aesar's Puratronic chemical line, with a reported purity of ≥99.99% (trace metal basis). As discussed in Supplemental Material, the α-HgS and β-HgS were found to contain 6 and 8 atom % Hg(0), respectively. All solid Hg reference materials were diluted with boron nitride (BN) and placed in Al sample holders sealed with Kapton® tape. EXAFS spectra of mercury reference materials were collected at both 77K and 298K to determine if the reference materials were contaminated with liquid Hg(0). Self-absorption corrections were carried out on the α-Hg(0) spectra using algorithms from both the Athena (22) and GR-xafsX software packages (23), and self-absorption effects were found to be minimal. Three individual EXAFS scans were averaged for all model compounds except for α-Hg(0), in which case 12 scans were averaged. The number of individual EXAFS scans averaged for the mine waste samples ranged between 6 and 18, depending on Hg concentration.

EXAFS Data Analysis

Data averaging, background subtraction, and data fitting were carried out using the SixPACK EXAFS analysis software package (24,25). A slightly different E_0 for the start of the spline was used in linear combination fitting compared to shell-by-shell fitting, which accounted for a shift in the data in *k*-space as seen when comparing spectra from Fig. S5 and all other EXAFS figures. Decomposition of Hg L_{III}-edge EXAFS spectra from field samples was accomplished by linear combination least squares fitting over a *k*-range of 3–9.5 $Å^{-1}$

using a library of EXAFS spectra taken at 298K for the reference materials mentioned above. We used the 298K reference spectra because of the presence of α-Hg(0) in the HgS reference materials (discussed below and in Supplemental Material); this approach minimized the Hg(0) contribution to the reference material EXAFS spectra, which would have complicated the linear combination fitting. The linear combination approach to decomposing EXAFS spectra has previously been shown to be effective for determining the identity and relative percentages of crystalline Hg-containing phases in Hg-polluted sediments (17). At higher *k* values, the α-Hg(0) EXAFS spectrum has one maximum that is aligned with a maximum in the 298K cinnabar EXAFS spectrum at $k = 8.7$ and with a maximum in the 298K metacinnabar EXAFS spectrum at $k = 9.5$ (Fig. 2). These alignments result in the α-Hg(0) fraction being zero or negative when using the automated fitting protocol in SixPACK for samples that contain cinnabar, metacinnabar, and α-Hg(0) because of the heavier weighting given to the high-*k* portion of the EXAFS data in the automated fitting. To compensate for this problem, spectra were fit using the automated fitting protocol of SixPACK for all Hg species, excluding α-Hg(0), and then by manually adding the α-Hg(0) spectrum to the fit at increasing fractions of α-Hg(0). A residual was calculated (see below) for each increase in the α-Hg(0) fraction and plotted versus the percent of α-Hg(0) added (see Fig. S6 in Supplemental Material). The quality of fit was determined by calculating the residual of the fit versus the data using the following formula:

$$\text{Residual} = \frac{\sum_{t=1}^{n} (v_{\text{data}} - v_{\text{fit}})^2}{n}$$

where "v" is the k^3-weighted chi(k) value in the EXAFS spectra (for both the data and fit) and "n" is the number of data points in the fit. For samples containing α-Hg(0), the residuals plot as a parabola, whereas samples not containing α-Hg(0) showed a minimum at 0% α-Hg(0), as shown in Figures S6 (Supplemental Materials). For details of the sample fitting protocol see Supplemental Material.

Previous use of linear combination fitting of Hg L_{III}-edge EXAFS spectra for mixtures of Hg model compounds has shown an accuracy of ~5% to ~10% in quantifying the percentages of Hg-bearing phases in two- and three-component systems, respectively (17). This method works well only when reference spectra used in the fitting procedure are significantly different in phases and amplitudes (see, *e.g.*, (26)). As shown by Kim *et al.* (17), this condition is met for EXAFS spectra of a number of Hg-containing reference materials, and as will be shown below, this is also true for the low-temperature EXAFS spectrum of α-Hg(0). Because liquid Hg(0) is difficult to homogenize in a mixture of solid phases, a two- or three-component test of the linear combination fitting approach using liquid Hg(0) has not been possible up to this point. However, because linear combination fitting of the Hg L_{III} EXAFS spectra of the "ultra-pure" α-HgS and β-HgS reference materials showed that they contain 6 atom% and 8 atom%, respectively, of Hg(0) (detailed discussion in Supplemental Material), we were able to assess the accuracy of this approach for liquid Hg(0)-containing samples. The other Hg-containing reference materials were found to have undetectable amounts of liquid Hg(0). Linear combination fitting of the low-temperature EXAFS spectra of the Hg(0)-containing α-HgS and β-HgS reference materials (Fig. S4 in Supplemental Material, plotted using lower E_0 for consistency) showed that an accuracy of ~5% can also be obtained when this liquid phase is crystallized. Therefore, we estimate that our linear combination fitting results for Hg L_{III}-edge EXAFS spectra of field samples have an accuracy of ~5% of the phases detected, including Hg(0).

To confirm the formation of α-Hg(0) in our slow cooling protocol, we compared the experimental low temperature EXAFS spectrum of our α-Hg(0) sample with theoretical EXAFS spectra generated using FEFF8.2 (27) and the structure of α-Hg(0) reported by Barrett (28). The α-Hg(0) model used for FEFF pathway generation was created using the CrystalMaker software package (29) and crystallographic data for α-Hg(0) from Barrett (28), who specified only the crystal system (rhombohedral) but not the space group symmetry. Therefore, all seven possible rhombohedral space groups (R3, R$\bar{3}$, R32, R3m, R3c, R$\bar{3}$m, and R$\bar{3}$c) were tested for α-Hg(0) using CrystalMaker (29), and the d-spacings of the resulting structures generated using CrystalDiffract (30) were compared with the experimental d-spacings for α-Hg(0) reported by Barrett (28) (results in Supplemental Material). The R$\bar{3}$m structure was chosen as the correct one, based on this comparison, although the R3 and R3m structures provided equally good fits between experiment and theory. We also compared Hg-Hg distances and multiple scattering pathways derived from fits of the experimental 77K EXAFS spectrum of α-Hg(0) with those derived by fitting the theoretical EXAFS spectrum of the R$\bar{3}$m α-Hg(0) structure derived using FEFF 8.2 (see Fig. S1 in Supplemental Material). In this fitting, single- and multiple-scattering pathways were generated for α-Hg(0) using FEFF 8.2, with a self-consistency function included to better fit the pure metal spectrum (27). Again, this comparison indicates that the R$\bar{3}$m (or R$\bar{3}$ or R3m) α-Hg(0) structure provides the best fit between experiment and theory.

Results and Discussion

Mercury Speciation in Mine Waste and Sediment Samples

Previous speciation studies of mercury in Hg mine waste and sediments based on ambient-temperature EXAFS studies (7,17) resulted in the finding of relatively insoluble HgS species being dominant in all samples examined, with minor amounts of water-soluble phases such as montroydite (HgO), schutteite ($Hg_3(SO_4)O_2$), eglestonite ($Hg_6Cl_3O(OH)$), corderoite ($Hg_3S_2Cl_2$), and $HgCl_2$. To properly fit the Hg L_{III}-edge EXAFS spectra of natural samples collected at 77K with light:dark Hg flux ratios greater than ~3.5, it was necessary to include the α-Hg(0) reference spectrum in the least squares fitting. The addition of α-Hg(0) resulted in a minimization of fit residuals in a statistically significant fashion based on Hamilton's R-factor ratio test (31) (see Supplemental Material). Plots of EXAFS spectra for all 8 samples are shown in Fig. S5 and the fit residuals are plotted in Fig. S6 (Supplemental Material). Fits of all the spectra taken at 77K are in reasonable agreement with the results of ambient-temperature EXAFS studies, except that the ambient-temperature speciation data did not include α-Hg(0) (Table 1). Results of linear combination fitting of EXAFS spectra of slowly cooled samples taken at 77K resulted in the detection of significant concentrations (9 to 22 atom%) of elemental Hg in five of the eight samples (Table 1). The low-temperature EXAFS spectra are superior to ambient-temperature spectra for linear combination fitting of EXAFS spectra of Hg mine wastes because of the superior signal-to-noise ratios of the former, the damped thermal motion of atoms in the samples at 77K, and the ability to detect liquid Hg(0) using the low temperature sample preparation protocol and 77 K EXAFS.

Correlation Between Hg Speciation and Evasion

Results from mercury evasion studies of the eight Hg mine field samples used in the present study show differences between silica-carbonate- and hot springs-type deposits, but no clear trend between Hg fluxes under both light and dark exposures and total Hg concentration is discernable for these eight samples (Table 1 and Fig. 3A). Earlier EXAFS studies at ambient-temperature had difficulty explaining differences in light:dark Hg fluxes of these samples when HgS minerals were the only dominant Hg phases detected. Gustin *et al.* suggested that photoreduction of Hg sulfide- and Hg chloride-containing phases along with

Hg bound to organics and Fe oxides could produce Hg(0) (32,33). These earlier studies also noted that photoreduction and/or physical desorption of Hg(0) is important.

A number of variables can affect the rate of mercury evasion from Hg-contaminated samples. For example, several groups have shown that soil moisture, temperature, atmospheric Hg concentrations, and light have strong impacts on Hg volatilization rates (34–36). The samples used in our experiments were dried at room-temperature before volatilization experiments were conducted, making the soil moisture and atmospheric Hg concentrations of little consequence in this study. Since the Pyrex sample chamber used in the flux chambers did not transmit light of wavelength < 500nm, exposure of the samples to UV light is not the cause of the enhancement of Hg volatilization (32). Because the penetration depth of light of wavelength >500nm into sediment grains is 50–100μm in most soils (37), it is likely that Hg fluxes should decrease over time as exposed sediments become depleted in liquid Hg(0). However, movement of gaseous elemental Hg by diffusion towards the surface (38,39), in addition to sediment turnover from slope failure, winter rain run-off, and/or aeolian processes, could expose new material containing Hg(0) to sunlight, resulting in more or less continuous gaseous Hg volatilization over time.

We found that in samples with light:dark Hg flux ratios >3.5 α-Hg(0) comprised between 9% and 22% of the total Hg species (Table 1), whereas in those samples with light:dark Hg flux ratios < 3.5 there was no detectable Hg(0) based on EXAFS linear combination fitting. When light:dark Hg flux ratio is plotted versus % liquid Hg(0), linear relationships emerge for both silica-carbonate- and hot springs-type Hg deposits (Fig. 3B). The trends in Fig. 3B offer another reason for differences in Hg evasion rates from different mine waste samples, which is the presence of relatively abundant liquid Hg(0) (up to 22 atom%) in some mercury mine wastes, part of which is native and not the result of photoreduction of higher valent Hg species.

In the California Coast Range, silica-carbonate deposits were formed by alteration of serpentinite rocks, which tended to result in Hg-bearing minerals of larger crystal size when compared with the younger hot springs-type deposits (2). A possible explanation for the lower slope of the silica-carbonate-type trend relative to the hot springs-type trend (Fig. 3B) is that Hg(0) globules are generally larger in silica-carbonate-type Hg deposits (or are entrained/encapsulated within larger particles) and thus limit Hg(0) evasion to the atmosphere relative to the smaller Hg(0) globules in hot springs-type deposits. Consistent with this explanation is Sladek and Gustin's observation that less Hg(0) volatilized during pyrolysis of larger Hg(0) beads relative to smaller beads (13). The higher Hg(0) concentrations observed in hot springs-type relative to silica-carbonate-type deposits (Fig. 3B) may be related to the generally smaller grain size of Hg-containing minerals from hot springs-type deposits (Rytuba, pers. comm.), which should make them more susceptible to weathering and conversion into liquid Hg(0). Another explanation for this observation is that the higher chloride content in both HgS crystals and hydrothermal solutions in hot springs-type Hg deposits leads to enhanced photosensitivity of HgS crystals, which should result in higher levels of Hg(0) produced by photoreduction (19,40,41). Although liquid Hg(0) globules were not detected in Sulphur Bank samples by Varekamp and Buseck (*42*), liquid Hg(0) is clearly present in large concentrations (up to 22 atom %), and, as a consequence, Sulphur Bank samples have the largest light:dark Hg flux ratio relative to the other samples examined in the present study.

Implications of Low-temperature Hg L_{III}-edge EXAFS Spectroscopy for Hg Evasion Data

Using low-temperature EXAFS spectroscopy and a new sample cooling protocol, we have shown that a significant amount of liquid Hg(0) (up to 22 atom %), previously undetectable by conventional EXAFS spectroscopy methods, is present in mercury mining wastes

associated with abandoned Hg mines in the California Coast Range. The speciation data obtained using this new approach help explain the higher light:dark Hg flux ratios from Hg mine wastes and sediment samples containing higher concentrations of liquid Hg(0). However, complete understanding of Hg evasion rates has not yet been achieved because only a limited number of samples have been studied to date using these new experimental protocols. Additional Hg speciation *vs*. light:dark Hg flux ratio data are needed to verify the two linear correlations seen in Fig. 3B, and such studies are underway. Based on the present study, however, it is clear that previous ambient-temperature EXAFS analyses of Hg-impacted sediments and mine wastes do not result in a complete picture of Hg cycling in Hg mining environments because the concentration of liquid Hg(0) is missing from the speciation information.

Supplementary Material

Refer to Web version on PubMed Central for supplementary material.

Acknowledgments

We wish to thank Joe Rogers and John Bargar of the Stanford Synchrotron Radiation Lightsource for help with data collection on beamline 11-2. The LN_2 cryostat used in the low-temperature work was designed and built by Steve Conradson of Los Alamos National Laboratory. GEB thanks George Parks (Stanford University) for helpful discussions over a number of years about the environmental chemistry of mercury. Funding for this research comes from the Stanford Environmental Molecular Science Institute through NSF Grant CHE-0431425. Portions of this research were carried out at the Stanford Synchrotron Radiation Lightsource, a National user facility operated by Stanford University on behalf of the U.S. Department of Energy, Office of Basic Energy Science, with additional support from the National Institute of Health.

Literature Cited

1. Ullrich SM, Tanton TW, Abdrashitova SA. Mercury in the aquatic environment: A review of factors affecting methylation. Critical Reviews in Environmental Science and Technology. 2001; 31(3): 241–293.
2. Rytuba JJ. Mercury from mineral deposits and potential environmental impact. Environmental Geology. 2003; 43:326–338.
3. Hylander LD. Global mercury pollution and its expected decrease after a mercury trade ban. Water, Air, and Soil Pollution. 2001; 125:331–344.
4. Morel FMM, Kraepiel AML, Amyot M. The chemical cycle and bioaccumulation of mercury. Annual Review of Ecological Systems. 1998; 29:543–566.
5. Bloom NS, Preus E, Katon J, Hiltner M. Selective extractions to assess the biogeochemically relevant fractionation of inorganic mercury in sediments and soils. Analytica Chimica Acta. 2003; 479(2):233–248.
6. Biester H, Scholz C. Determination of mercury binding forms in contaminated soils: Mercury pyrolysis versus sequential extractions. Environmental Science & Technology. 1997; 31(1):233–239.
7. Kim CS, Rytuba JJ, Brown GE Jr. Geological and anthropogenic factors influencing mercury speciation in mine wastes: An EXAFS spectroscopy study. Applied Geochemistry. 2004; 19:379–393.
8. Skyllberg U, Bloom PR, Qian J, Lin C-M, Bleam WF. Complexation of mercury(II) in soil organic matter: EXAFS evidence for linear two-coordination with reduced sulfur groups. Environmental Science & Technology. 2006; 40(13):4174–4180. [PubMed: 16856732]
9. Skyllberg U, Qian J, Frech W. Combined XANES and EXAFS study on the bonding of methyl mercury to thiol groups in soil and aquatic organic matter. Physica Scripta. 2005; T115:894–896.
10. Kim CS, Bloom NS, Rytuba JJ, Brown GE Jr. Mercury speciation by x-ray absorption fine structure spectroscopy and sequential chemical extractions: A comparison of speciation methods. Environmental Science & Technology. 2003; 37(22):5102–5108. [PubMed: 14655695]

11. Lowry GV, Shaw S, Kim CS, Rytuba JJ, Brown GE Jr. Macroscopic and microscopic observations of particle-facilitated mercury transport from New Idria and Sulphur Bank Mercury Mine tailings. Environmental Science & Technology. 2004; 38(19):5101–5111. [PubMed: 15506205]
12. Sladek C, Gustin MS, Kim CS, Biester H. Application of three methods for determining mercury speciation in mine waste. Geochemistry: Exploration, Environment, Analysis. 2002; 2:369–376.
13. Sladek C, Gustin MS. Evaluation of sequential and selective extraction methods for determination of mercury speciation and mobility in mine waste. Applied Geochemistry. 2003; 18:567–576.
14. Biester H, Gosar M, Covelli S. Mercury speciation in sediments affected by dumped mining residues in the drainage area of the Idrija Mercury Mine, Slovenia. Environmental Science & Technology. 2000; 34(16):3330–3336.
15. Biester H, Gosar M, Muller G. Mercury Speciation in tailings of the Idrija Mercury Mine. Journal of Geochemical Exploration. 1999; 65:195–204.
16. Biester H, Nehrke G. Quantification of mercury in soils and sediments-acid digestion versus pyrolysis. Fresenius' Journal of Analytical Chemistry. 1997; 358:446–452.
17. Kim CS, Brown GE Jr, Rytuba JJ. Characterization and speciation of mercury-bearing mine wastes using x-ray absorption spectroscopy. The Science of the Total Environment. 2000; 261:157–168. [PubMed: 11036987]
18. Slowey AJ, Rytuba JJ, Brown GE Jr. Speciation of mercury and mode of transport from placer gold mine tailings. Environmental Science & Technology. 2005; 39(6):1547–1554. [PubMed: 15819208]
19. Gustin MS, Biester H, Kim CS. Investigation of the light-enhanced emission of mercury from naturally enriched substrates. Atmospheric Environment. 2002; 36:3241–3254.
20. U.S. Environmental Protection Agency. Method 1631, Revision E: Mercury in water by oxidation, purge and trap, and cold vapor atomic fluorescence spectrometry. EPA; Washington, DC: 2002.
21. Thermal and mechanical properties of Teflon (polytetra fluorethylene). [accessed Feb 2, 2009]. www.yutopian.com/Yuan/prop/Teflon.html
22. Ravel, B. Athena, version 0.8.056. 2002.
23. Farges, F. GR-xafsX, version 2.4. 2008.
24. Webb, S. SixPACK, version 0.67. Stanford Synchrotron Radiation Lightsource; Menlo Park, CA: 2006.
25. Webb SM. SixPACK: a graphical user interface for XAS analysis using IFEFFIT. Physica Scripta. 2005; T115:1011–1014.
26. Catalano JG, Brown GE Jr. Analysis of uranyl-bearing phases by EXAFS spectroscopy: Interferences, multiple scattering, accuracy of structural parameters, and spectral differences. Am Mineral. 2004; 89:1004–1021.
27. Ankudinov AL, Ravel B, Rehr JJ, Conradson SD. Real-space multiple-scattering calculation and interpretation of x-ray-absorption near-edge structure. Physica Review B. 1998; 58(12):7565–7576.
28. Barrett CS. The structure of mercury at low temperatures. Acta Crystallogr. 1957; 10:58–60.
29. Palmer, D.; Conley, M. CrystalMaker for Windows version 2.0.7. CrystalMaker Software Ltd; 2008.
30. Palmer, D.; Conley, M. CrystalDiffract for Windows version 1.1.2. CrystalMaker Software Ltd; 2007.
31. Hamilton WC. (1965) Significance test on the crystallographic R factor. Acta Crystallogr. 1965; 18(3):502–510.
32. Gustin, MS.; Nacht, D.; Engle, MA. Speciation of mercury above naturally and anthropogenically mercury enriched substrate. Abstract with Program, American Chemical Society National Meeting; 2002.
33. Gustin MS. Are mercury emissions from geologic sources significant? A status report. The Science of the Total Environment. 2003; 304:153–167. [PubMed: 12663180]
34. Moore C, Carpi A. Mechanisms of the emission of mercury from soil: Role of UV radiation. Journal of Geophysical Research. 2005; 110(D24302):1–9.

35. Xin M, Gustin MS, Johnson D. Laboratory investigation of the potential for re-emission of atmospherically derived Hg from soils. Environmental Science & Technology. 2007; 41(14): 4946–4951. [PubMed: 17711207]

36. Xin M, Gustin MS. Gaseous elemental mercury exchange with low mercury containing soils: Investigation of controlling factors. Applied Geochemistry. 2007; 22:1451–1466.

37. Ciani A, Goss KU, Schwarzenbach RP. Light penetration in soil and particulate minerals. European Journal of Soil Science. 2005; 56:561–574.

38. Zhang H, Lindberg SE. Processes influencing the emission of mercury from soils: A conceptual model. Journal of Geophysical Research. 1999; 104(D17):21889–21896.

39. Gustin MS, Stamenkovic. Effect of watering and soil moisture on mercury emissions from soils. Biogeochemistry. 2005; 76:215–232.

40. McCormack JK. The darkening of cinnabar in sunlight. Mineralium Deposita. 2000; 35:796–798.

41. Varekamp JC, Buseck PR. The speciation of mercury in hydrothermal systems, with applications to ore deposition. Geochimica et Cosmochimica Acta. 1984; 48(1):177–185.

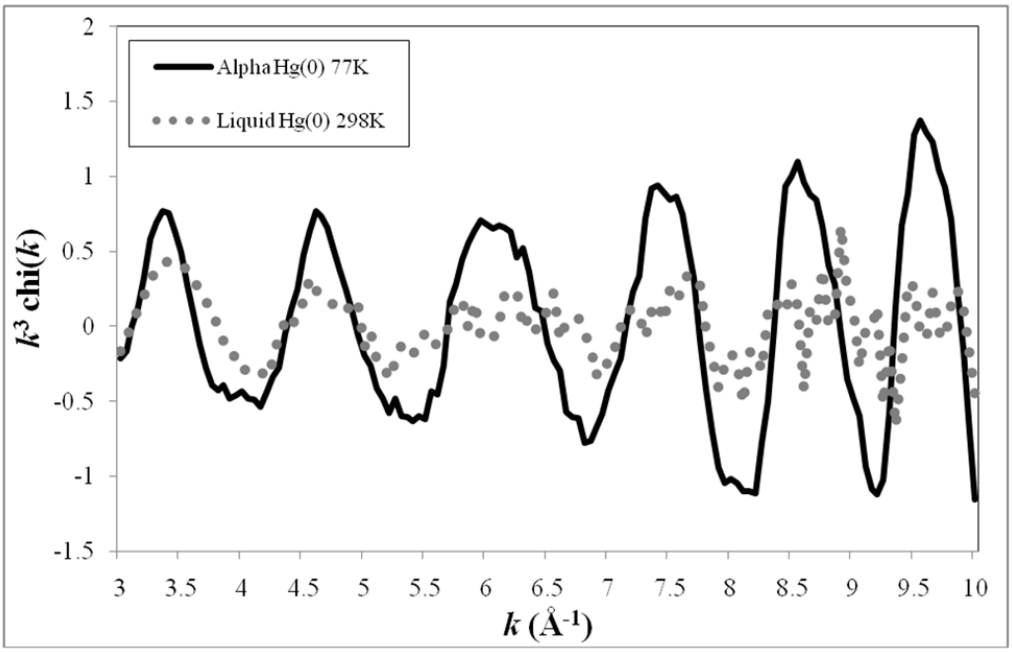

Figure 1.
Hg L_{III} EXAFS spectra for elemental Hg(0) at room temperature (liquid Hg(0)) and 77K (α-Hg(0)) showing the enhancement of amplitudes in the Hg L_{III} EXAFS spectrum obtained at 77K after slow cooling of the sample. These spectra were averaged from 12 scans each.

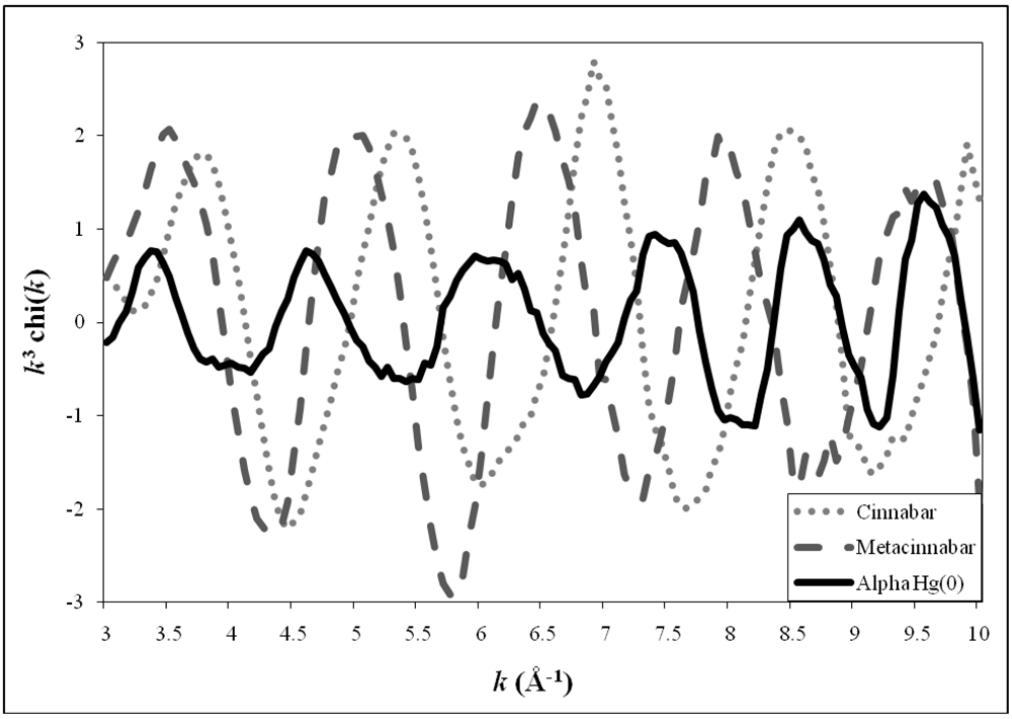

Figure 2.

Comparison of k^3-weighted Hg L_{III}-EXAFS spectra of α-Hg(0), α-HgS, and β-HgS. The α-Hg(0) spectrum was taken at 77K, whereas α-HgS and β-HgS spectra were taken at 298K. The α-Hg(0) sample was prepared using the new sample cooling protocol discussed in the text.

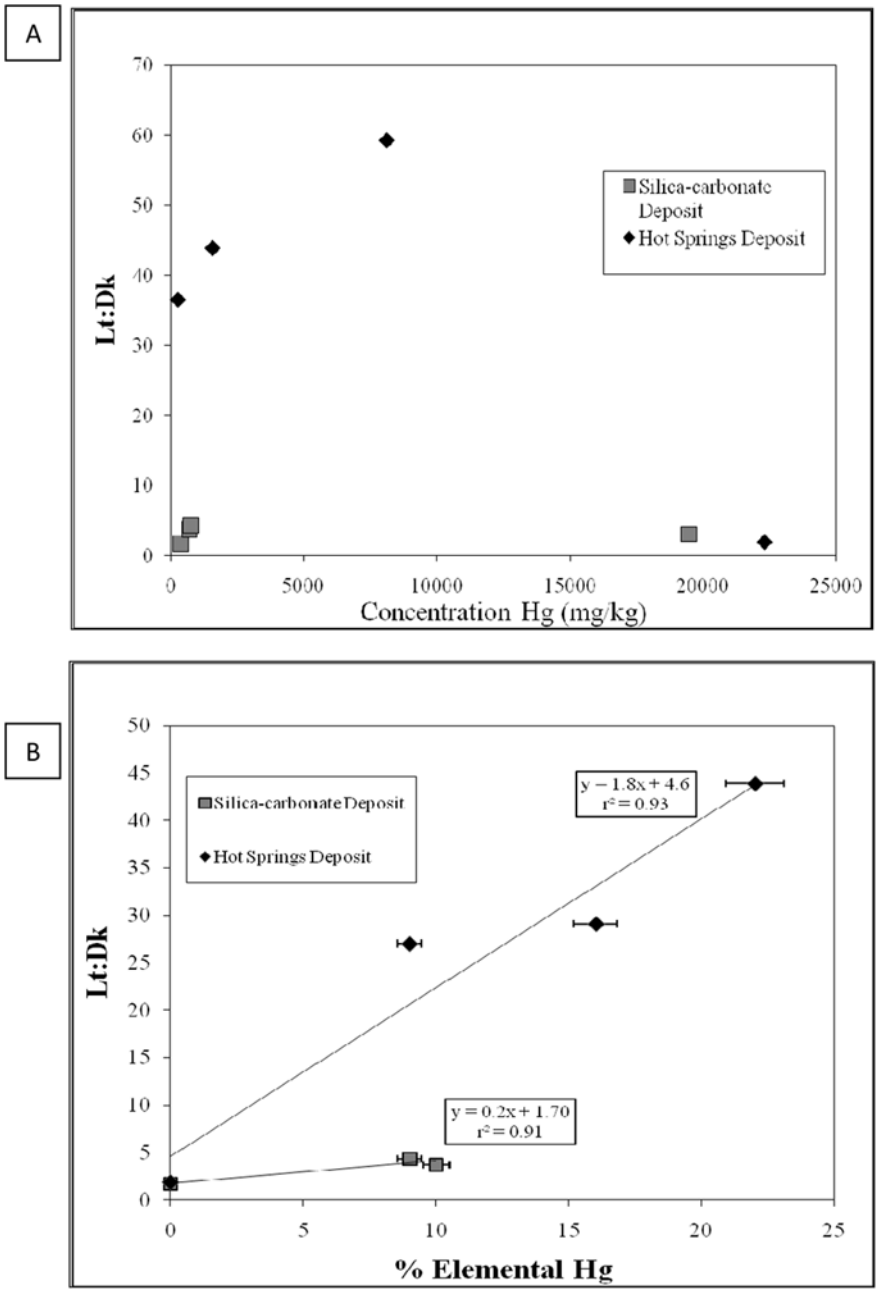

Figure 3.

(A) Plot of light:dark evasion data versus total Hg concentration for silica-carbonate and hot springs deposits. **(B)** Plot of light:dark (Lt:Dk) evasion data versus % liquid Hg(0) in each sample, with data points grouped into silica-carbonate and hot springs deposits. Plot B shows the linear relationship between Lt:Dk and % liquid Hg(0) for the two separate deposit types. y-intercepts not equaling 1 are considered to be the result of encapsulation of liquid Hg(0) in sediment grains. Lt:Dk error bars are smaller than the symbols used.

Table 1

Sample information for selected Hg-mine sediments including results from Hg evasion studies and low-temperature EXAFS analysis, including linear combination EXAFS fitting results, compared with ambient-temperature linear combination EXAFS fitting results. The estimated accuracies of the linear combination fit results in the column labeled "**Hg Speciation (77K)**" are ±5%. α-HgS = cinnabar; β-HgS = metacinnabar

Sample Name	Location (deposit type)	Sample Type	Hg Concentration (ppm)	Light Hg Flux @35°C (ng/m2h)	Dark Hg Flux @35°C (ng/m2h)	light:dark ratio	Hg Speciation (298K)	Hg Speciation (77K)	Residual (77K)
KN1B	Knoxville (hot springs)	Calcine	277	2257 ± 50	78 ± 19	36.0 ± 0.2	22% α-HgS 78% β-HgS	32% α-HgS 52% β-HgS 16% Hg(0)	0.381
NISB	New Idria (silica-carbonate)	Calcine (500–2000 μm)	350	20857 ±160	12307 ± 307	1.7 ± 0.1	34% α-HgS 43% β-HgS 23% Eglestonite	36% α-HgS 47% β-HgS 17% Eglestonite	0.09
NIS3	New Idria (silica-carbonate)	Calcine (75–125 μm)	690	14390 ± 450	3874 ± 148	3.7 ± 0.1	29% α-HgS 56% β-HgS 15% Montroydite	35% α-HgS 48% β-HgS 7% Montroydite 10% Hg(0)	0.099
NIS6	New Idria (silica-carbonate)	Calcine (<45 μm)	770	15778 ± 131	3655 ± 381	4.3 ± 0.1	56% α-HgS 44% β-HgS	45% α-HgS 46% β-HgS 9% Hg(0)	0.061
SBW9 S3	Sulphur Bank (hot springs)	Waste Rock (500–2000 μm)	1580	4301±336	98 ± 14	43.9 ± 0.2	65% α-HgS 35% β-HgS	48% α-HgS 30% β-HgS 22% Hg(0)	0.126
SBW9 S6	Sulphur Bank (springs)hot	Waste Rock (75–125 μm)	22310	7334±173	3851 ± 114	1.9 ± 0.1	82% α-HgS 18% β-HgS	81% α-HgS 19% β-HgS	0.168
SBW9 S9	Sulphur Bank (hot springs)	Waste Rock (<45 μm)	8120	9032±176	334 ± 212	27.1 ± 0.1	78% α-HgS 22% β-HgS	61% α-HgS 30% β-HgS 9% Hg(0)	0.12
NAC3	New Almaden (silica-carbonate)	Condenser Soot	19500	46586± 946	15058 ± 2614	3.1 ± 0.2	100% β-HgS	100% β-HgS	0.051